Available online at www.sciencedirect.com
SCIENCE DIRECT®
Combustion and Flame 143 (2005) 159–173
Combustion and Flame
www.elsevier.com/locate/combustflame

Liftoff characteristics of partially premixed flames under normal and microgravity conditions

Andrew J. Lock [a], Alejandro M. Briones [a], Xiao Qin [b], Suresh K. Aggarwal [a,*], Ishwar K. Puri [c], Uday Hegde [d]

[a] *Department of Mechanical and Industrial Engineering, University of Illinois at Chicago, Chicago, IL 60607, USA*
[b] *Department of Mechanical & Aerospace Engineering, Princeton University, Princeton, NJ 08544, USA*
[c] *Department of Engineering Science and Mechanics, Virginia Polytechnic Institute and State University, Blacksburg, VA 24061, USA*
[d] *National Center for Microgravity Research, Cleveland, OH 44135, USA*

Received 1 November 2004; received in revised form 29 April 2005; accepted 11 May 2005

Available online 28 July 2005

Abstract

An experimental and computational investigation on the liftoff characteristics of laminar partially premixed flames (PPFs) under normal (1-g) and microgravity (μ-g) conditions is presented. Lifted methane–air PPFs were established in axisymmetric coflowing jets using nitrogen dilution and various levels of partial premixing. The μ-g experiments were conducted in the 2.2-s drop tower at the NASA Glenn Research Center. A time-accurate, implicit algorithm that uses a detailed description of the chemistry and includes radiation effects is used for the simulations. The predictions are validated through a comparison of the flame reaction zone topologies, liftoff heights, lengths, and oscillation frequencies. The effects of equivalence ratio, gravity, jet velocity, and radiation on flame topology, liftoff height, flame length, base structure, and oscillation frequency are characterized. Both the simulations and measurements indicate that under identical conditions, a lifted μ-g PPF is stabilized closer to the burner compared with the 1-g flame, and that the liftoff heights of both 1-g and μ-g flames decrease with increasing equivalence ratio and approach their respective nonpremixed flame limits. The liftoff height also increases as the jet velocity is increased. In addition, the flame base structure transitions from a triple- to a double-flame structure as the flame liftoff height decreases. A modified flame index is developed to distinguish between the rich premixed, lean premixed, and nonpremixed reaction zones near the flame base. The 1-g lifted flames exhibit well-organized oscillations due to buoyancy-induced instability, while the corresponding μ-g flames exhibit steady-state behavior. The effect of thermal radiation is to slightly decrease the liftoff heights of both 1-g and μ-g flames under coflow conditions.

Keywords: Flame liftoff; Partial premixing; Microgravity; Flame stabilization; Diluents; Flame index

* Corresponding author. Fax: +1 312 413 0441.
E-mail address: ska@uic.edu (S.K. Aggarwal).

0010-2180/$ – see front matter
doi:10.1016/j.combustflame.2005.05.011

1. Introduction

Partially premixed flames (PPFs) are established by flowing a fuel-rich gas stream adjacent to a fuel-lean stream. The associated concentration gradients support flames with multiple reaction zones. In general, a rich premixed flame is established in the fuel-rich zone, and a nonpremixed flame, outside of this region. Often a lean premixed flame is also established in the fuel-lean region. Then, the nonpremixed flame is located between the rich and lean premixed flames. PPFs can be described as hybrid flames with the characteristics of both nonpremixed and premixed flames. Consequently, using partial premixing, one can exploit the advantages of both nonpremixed and premixed flames with respect to safety, emissions control, and flame stability [1,2]. A detailed understanding of the structure of PPFs is important from both practical and scientific considerations. These flames occur in numerous combustion systems including gas-fired domestic burners and industrial furnaces, as well as in spray combustion systems, such as gas turbines [3] and diesel engines [4], in which the vaporization of smaller droplets and/or poor mixing lead to locally fuel vapor-rich regions [5]. It is important therefore to gain a fundamental understanding of the structure and liftoff characteristics of PPFs.

Partially premixed combustion is also important in space applications, particularly due to fire safety considerations [6,7]. Previous studies have shown that the structure of PPFs can be modified significantly by changing the level of partial premixing and buoyancy [8,9]. As fires represent uncontrolled combustion, it is difficult to categorize them in terms of premixed or nonpremixed flames. There is good likelihood that fires can originate in partially premixed mode, when a pyrolyzed or evaporated fuel forms an initial fuel-rich mixture with the ambient air. Such scenarios are relevant for fires both on earth and in hypogravity environments. Because most previous research on fires has focused on either premixed or nonpremixed flames, it is important to investigate PPFs in the context of fire safety under different gravity conditions. The complex convective-diffusive transport processes that mix the fuel with air, heat the mixture, and facilitate burning are significantly modified by buoyant environment. Therefore, a detailed investigation of the structure and stability of microgravity flames can enhance our understanding of combustion in both earth and space environments so that we can better address harmful combustor emissions, fuel efficiency, and fire safety and suppression. Flame extinguishment techniques commonly involve the suppression of a flame by use of a diluent. While the absolute extinguishment concentrations for various diluents and the flame behavior prior to extinguishment are reasonably well characterized for a variety of configurations, the behavior of lifted flames prior to their blowout under microgravity (μ-g) conditions is not yet fully known. Consequently, it is important to investigate the effect of gravity on the liftoff characteristics of PPFs due to fire safety considerations in space.

Flame stabilization and liftoff are complex processes involving transport, partial premixing, ignition, and extinction. Peters and Williams [10] and Pitts [11] have provided reviews on theories of turbulent diffusion flame stabilization. Lifted flames in laminar nonpremixed jets have been extensively investigated to gain a fundamental understanding of the liftoff and stabilization phenomena [12–17]. These investigations have observed that lifted flames often have a triple or tribrachial flame structure at their base. Chung and Lee [12,13] reported that for nonpremixed laminar jets, propane and *n*-butane flames can become lifted, while methane and ethane flames blow out directly from a burner-stabilized mode. Their analysis showed that the Schmidt number Sc plays an important role in flame liftoff. Stable lifted flames are possible only for fuels for which Sc is greater than 1 or less than 0.5. Kioni et al. [14], and Plessing et al. [18] established lifted triple flames using nitrogen-diluted methane fuel and investigated the effect of strain rate. Ghosal and Vervisch [16] demonstrated analytically that a lifted laminar flame is possible for a fuel for which Sc is greater than a critical value Sc_{cr}, where Sc_{cr} can be less than unity. For values of $Sc < Sc_{cr}$, they showed that a lifted flame is subcritical and can survive only in a narrow parametric region.

The lifted flames in these investigations were stabilized in the far field of a jet, with the liftoff heights being of the order of 10 cm. This allowed additional fuel–air mixing in the upstream region and, thereby, the formation of a triple-flame structure at the flame base. These lifted flames are characterized by a flame propagation speed such that a flame is stabilized where the flame speed equals the local flow velocity along the stoichiometric mixture fraction line. The flame propagation speed, however, differs from the corresponding unstretched laminar speed due to the effects of curvature and flow divergence upstream of the flame base or the triple point. Echekki and Chen [19] concluded from direct numerical simulations that both curvature and diffusion effects augment radical production that enhances the flame propagation speed. Previous experimental and computational investigations have identified the minimum flow speed located at the triple point as the premixed laminar flame speed, and distinguished it from the triple-flame propagation speed, which is considered further upstream of the triple point, and is generally larger than the former [14,20–22].

The behavior of lifted flames that are stabilized near the burner exit (i.e., with liftoff heights that are typically smaller than 1 cm) can be expected to be different from the behavior of lifted flames established in the far field. Takahashi et al. [23] investigated the stabilization of nonpremixed flames and, instead of a triple-flame structure, they found the existence of a reaction kernel of high reactivity. This kernel provided radicals and served as a flame stabilization point in a small premixing zone. Kim et al. [24] examined liftoff characteristics with respect to fuel concentration gradients and noted that the flame liftoff height and propagation velocity can be controlled by varying the mixture concentration gradient. They found that as the concentration gradient was increased, the liftoff heights of both methane and propane triple flames first decreased and then increased, showing a minimum value at a critical concentration gradient corresponding to the maximum propagation velocity. They suggested that this critical concentration gradient represented a criterion for transition from a premixed flame to a triple flame.

Our literature review indicates that previous experimental and computational studies have focused mostly on the liftoff characteristics of nonpremixed flames. Except for the single experimental study reported by Kim et al. [24], the liftoff and stabilization characteristics of partially premixed flames have not been investigated, although such flames are relevant in numerous combustion systems. This provides the major motivation for our investigation, which focuses on the liftoff characteristics of partially premixed flames. Another motivation is due to the consideration that buoyancy is an important factor in lifted flame stabilization, and that PPFs are relevant from the perspective of fire safety in space. Buoyant acceleration not only influences the global flame structure and liftoff behavior through increased entrainment and lateral compression of the gas stream [12,13]; it can also induce well-organized, low-frequency oscillations in both burner-stabilized and lifted PPFs [12,25]. The repetitive interaction of burning rate and buoyancy-induced convection is responsible for lifted flame oscillations. Moreover, in the presence of buoyancy, it may be possible for a flame to stabilize in a flow with a velocity smaller than that of the laminar flame speed at the triple point [12]. These differences provide additional justification for investigating lifted PPFs under microgravity conditions.

The objective of this article is to experimentally and numerically investigate the liftoff characteristics of partially premixed flames under 1-g and μ-g conditions. Lifted methane–air PPFs are established in axisymmetric coflowing jets that are nitrogen diluted for various levels of partial premixing. A coflow configuration with equal jet and coflow velocities is employed to minimize the effects of the jet shear layer on the flame liftoff behavior. The μ-g experiments were conducted in the 2.2-s drop tower facility at the NASA Glenn Research Center. This is the first report of measurements of lifted PPFs in μ-g. The flames are simulated using a time-accurate, implicit algorithm that uses detailed descriptions of chemistry and transport. The effects of gravity, partial premixing (i.e., fuel stream equivalence ratio), inlet velocity, and radiation on the flame topology, liftoff height, flame length, base structure, and flame oscillation frequency are analyzed.

2. Experimental method

The μ-g experiments were conducted in the 2.2-s drop tower facility at the NASA Glenn Research Center in a self-contained drop rig. The rig is equipped with an axisymmetric coflowing burner. Equal jet and coflow velocities are employed so as to minimize the effects of jet shear layer on the flame structure and liftoff. Laminar flow conditions were maintained for all flames. A nearly flat top hat flow profile was established by including a series of screens inside the burner and at its exit. A schematic diagram of the burner and an image of the drop rig are provided in Fig. 1. The PPFs are established by introducing a rich methane–air mixture through the inner annulus and air through the outer annulus of the burner [1,2]. A “drop” involves the process of preparing the rig, filling and mixing gases in onboard cylinders, loading and raising the rig to the top of the tower, initiating recording devices and computer controls, stabilizing the flame in 1-g for a few seconds, dropping the rig to achieve μ-g, and thereafter retrieving it. Gas flow and ignition are initiated through timed computer controls and the flame is observed through remote video. The lifted flames are established at 1-g prior to the drop. Once the flame is stabilized in 1-g for a few seconds, the rig is released and the flame generally transitions into a μ-g state. The flame images are recorded at 30 frames per second by an onboard CCD camera and a tower-mounted Mini-DV recorder. No optical filters were used with the camera. The images presented are those of flame intensity mapped to a RGB pallet. Therefore, no specific reaction rate information can be derived from the images. A quantitative reaction rate measurement such as that of Najm et al. [26] was not possible due to equipment space limitations in the microgravity drop rig. The flames are lifted by diluting the fuel/air stream with 25% N_2 by volume. Measurements are obtained for ten cases with a matrix consisting of five equivalence ratios ($\phi = 2$, 2.25, 2.5, 2.75, 3) and two velocities ($V_{in}/V_{out} = 38$, 50 cm/s).

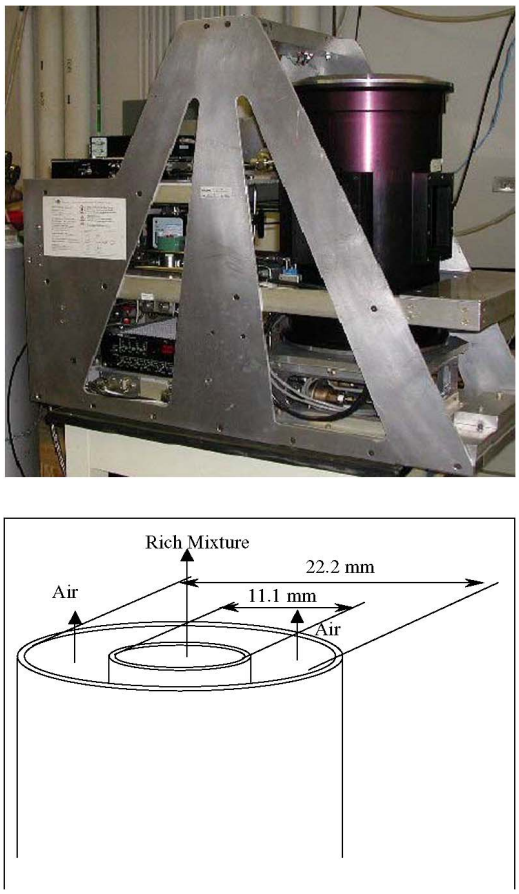

Fig. 1. Experimental setup. Top: UIC-NASA drop rig. Bottom: schematic of the coannular burner.

3. Numerical method

The computational model is based on the algorithm developed by Katta et al. [27] and the simulation method is described in detail elsewhere [1,2]. The numerical model solves the time-dependent governing equations for unsteady reacting flows in a two-dimensional planar or axisymmetric configuration. In axisymmetric coordinates, these equations are

$$\frac{\partial(\rho\Phi)}{\partial t}+\frac{\partial(\rho v\Phi)}{\partial r}+\frac{\partial(\rho u\Phi)}{\partial z}=\frac{\partial}{\partial r}\left(\Gamma^{\Phi}\frac{\partial\Phi}{\partial r}\right)+\frac{\partial}{\partial z}\left(\Gamma^{\Phi}\frac{\partial\Phi}{\partial z}\right)-\frac{\rho v\Phi}{r}+\frac{\Gamma^{\Phi}}{r}\frac{\partial\Phi}{\partial r}+S^{\Phi}.$$

Here, t denotes the time, and u and v represent the axial (z) and radial (r) velocity components, respectively. The general form of the equation represents conservation of mass, momentum, species, or energy conservation equation, depending on the variable used for Φ. The diffusive transport coefficient Γ^{Φ} and source terms S^{Φ} appearing in the above equation are provided in Table 1 of Ref. [1]. Introducing the overall species conservation equation and the state equation completes the set of equations. In addition, a sink term based on an optically thin gas assumption is included in the energy equation to account for thermal radiation from the flame [9]. The sink term due to the radiation heat loss is expressed as $q_{\mathrm{rad}}=-4\sigma K_{\mathrm{p}}(T^4-T_{\mathrm{o}}^4)$ [28], where T denotes the local flame temperature. The term K_{p} accounts for the absorption and emission from the participating gaseous species (CO_2, H_2O, CO, and CH_4) and is expressed as $K_{\mathrm{p}}=P\sum_k X_i K_{\mathrm{p},i}$ where $K_{\mathrm{p},i}$ denotes the mean absorption coefficient of the kth species. Its value is obtained by using a polynomial approximation to the experimental data provided in Ref. [13]. The methane–air chemistry is modeled using a detailed mechanism that considers 24 species and 81 elementary reactions [29]. The mechanism has been validated for the computation of premixed flame speeds and the detailed structure of both nonpremixed and partially premixed flames and PPFs [1,2,30–32].

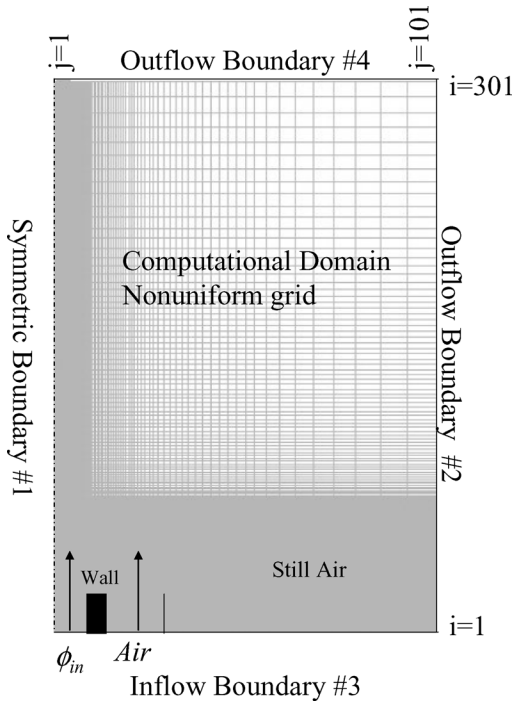

Fig. 2. Schematic of the computational domain and boundary conditions.

The computational domain of 150 × 100 mm^2 in the axial (z) and radial (r) directions, respectively, is represented by a staggered, nonuniform (301 × 101) grid system, as shown in Fig. 2. The reported results are grid independent. An isothermal insert simulates the inner 2 × 1-mm burner wall at 300 K. Atmospheric partially premixed methane–air flames were estab-

lished using an annular concentric burner that consists of a central tube with inner and outer diameters of 10.5 and 12.5 mm, respectively. This tube is surrounded by a concentric tube with inner and outer diameters of 22.2 and 25.2 mm, respectively. Methane–air fuel-rich mixtures and air were introduced from the inner and outer tubes, respectively. The velocity profile in the inner tube is assumed to be partially developed, while that in the outer tube is assumed to be uniform. These conditions were chosen to correspond as closely as possible to those in the experimental study. The boundary conditions used are:

1. *Symmetry boundary* (axis of symmetry): No fluxes are allowed to cross the symmetrical plane. The transverse velocity is set to zero at $J = 1$ (symmetry plane), while the values for all other variables are equal to those at $J = 2$.
2. *Outflow boundary in the transverse* (*or radial*) *direction*: There is a constant composition along this boundary with all velocities equal to zero.
3. *Inflow boundary*: This boundary is divided up into the inner annulus flow, the burner wall, the outer annulus flow and still air. The vertical and horizontal velocities, pressure, and temperature are assigned constant values along the boundary. The fuel and oxidizer mass fractions are different in each subdivision. The first inflow boundary corresponds to that for the inner jet issuing a rich methane–air mixture. The second inflow boundary describes the outer jet issuing air. The third inflow boundary corresponds to still air that has values equal to those for the outflow boundary in the radial direction.
4. *Outflow boundary in the axial direction*: This boundary allows the flow to exit the domain without being distorted. Therefore, the values at that boundary are computed from a weighted average of the values of the previous two axial grid points.

The outflow boundaries in both radial and axial directions are located sufficiently far from the respective symmetric and inflow boundaries to minimize boundary-induced disturbances.

4. Results and discussion

4.1. Validation of numerical model

Due to the complexities of microgravity research, the PPF drop rig currently has limited diagnostic capabilities. For this reason, numerical simulations are used for a more detailed investigation of the liftoff characteristics of PPFs. The numerical model has been previously validated for both burner-stabilized and lifted methane–air PPFs [2,25,33]. Additional validation is provided by comparing the predicted heat release and measured flame luminosity for 25% N_2-diluted lifted partially premixed flames at 1- and μ-g, as shown in Fig. 3. The flames were diluted with nitrogen to allow for their lifting. Absence of dilution or insufficient dilution resulted in burner-stabilized flames, as demonstrated by our simulations presented in Fig. 4a, which shows the topology (in terms of the heat release rate contours) of a burner-stabilized 1-g PPF established at $\phi = 2.0$, $V_{\text{in}} = V_{\text{out}} = 50$ cm/s, without nitrogen dilution.

The images of the 1- and μ-g lifted flames presented in Fig. 3a are from a color CCD camera. They have been converted into flame luminosity contours (also shown in the figure). Various methods of isolating specific spectral bands and relating them to a specific reaction rate intensity have been reported [1,2,26]. Specific reaction rate measurements were not possible in our experiments due to the constraints associated with the drop rig size, which prevented the use of an intensified CCD camera or a LIF system needed for such measurements. Both the original and processed images show a triple-flame structure at the flame base. Fig. 3b presents the corresponding predicted heat release rate contours (left) and the measured flame luminosity contours (right). The reaction rates are very large near the flame base. The peak values of the predicted heat release rate and the measured intensity are similar at the flame base, where the inner and outer reaction regions merge. Care is taken in comparing the 1-g flames at the same time, as they are subject to buoyancy-induced oscillations. The measured and predicted reaction zone topographies are in good agreement, as are the flame liftoff heights and lengths. Both the simulations and measurements show that in the absence of gravity, both the liftoff and flame heights decrease. Our previous work has shown that flames of this type are nearly fully developed in 2.2 s of μ-g [9]. Although the temperature field continues to evolve, the heat release rate profile shows insignificant change beyond 2.2 s.

4.2. Modified flame index

Previous investigations have distinguished the various reaction zones in PPFs based on their spatial locations [8,30]. In lifted flames, however, the premixing ahead of the flame front can be relatively small depending on the liftoff height. Consequently, it can be difficult to distinguish the reaction zones visually. To spatially resolve the various reaction zones in the lifted PPFs more clearly, we have developed a method based on a modified flame index. Takeno and coworkers [34] have suggested the use of such an index based on the scalar product of the gradients of fuel and oxidizer mass fractions, which distinguishes be-

tween the premixed and nonpremixed reaction zones. Their flame index is defined as [34]

$$G_{FO} = \nabla Y_F \cdot \nabla Y_O.$$

Here, Y_F denotes the fuel mass fraction and Y_O the oxidizer mass fraction. Domingo et al. [35], in their study of partially premixed gaseous and spray flames, normalized this flame index as

$$\xi_p = \frac{1}{2}\left(1 + \frac{G_{FO}}{|G_{FO}|}\right),$$

such that $\xi_p = 1$ and 0 represent the premixed and nonpremixed reaction zones, respectively. In our investigation, we modified the Domingo et al. [35] flame index based on the local mixture fraction such that it can also distinguish between the rich and lean premixed reaction zones.

It is well known that the stoichiometric mixture fraction f_S lies within the nonpremixed reaction zone [36]. Therefore, the rich and lean premixed zones are located in the inner and outer regions in which the local mixture fraction f is larger and smaller than f_S, respectively. Accordingly, we can define a modified flame index:

$$\xi_M = \left(\frac{f - f_S}{|f - f_S|}\right) \cdot \frac{1}{2}\left(1 + \frac{G_{FO}}{|G_{FO}|}\right).$$

Here, the mixture fraction is defined following Bilger [37]. With this definition $\xi_M = 1$ for the rich premixed zone, -1 for the lean premixed zone, and ± 0.5 or 0 (depending on the fuel under consideration) for the nonpremixed zone. If the fuel is completely consumed in the premixed zones, which is normally the case for PPFs burning hydrocarbon fuels [1,2,32], $\xi_M = \pm 0.5$, with $+0.5$ and -0.5 values corresponding to the nonpremixed regions adjacent to the rich premixed and lean premixed zones, respectively. The value of $\xi_M = 0$ for PPFs burning hydrogen, because the fuel is partially consumed in the premixed reaction zone, with the remaining fuel being consumed in the nonpremixed zone [38]. Identification of the various reaction zones is relevant only in regions of high reactivity, i.e., where the heat release rates are significant. Therefore, we have computed the flame index only in regions where the heat release rate is at least 1% of the maximum heat release rate.

The use of the modified flame index to identify different reaction zones in a PPF is illustrated in Fig. 4, which presents the predicted heat release rate and flame index contours for a 1-g PPF established at $\phi_{in} = 2.0$, $V_{in} = V_{out} = 50$ cm/s, with no nitrogen dilution. In the absence of dilution the PPF is stabilized at the burner and contains only two reaction zones, namely, the rich premixed zone and the nonpremixed zone. These two zones are readily identified by the flame index contours presented in Fig. 4b. The heat release rate contours also indicate that the PPF at 1-g is subjected to buoyancy-induced oscillations, which is discussed in a later section. Comparison of two 1-g PPFs established under identical conditions, one undiluted and the other with 25% nitrogen dilution, shows that the diluted and lifted flame possesses a triple-flame structure (cf. Fig. 3), while the undiluted flame is burner stabilized with a double-flame structure at the flame base.

4.3. Effect of partial premixing on liftoff height

Fig. 5 presents the measured flame luminosity contours for N_2-diluted 1- and μ-g-lifted PPFs for several equivalence ratios. The corresponding images of the simulated flames are presented in Fig. 6 in terms of the heat release rates, velocity vectors, and stoichiometric mixture fraction contours. The maximum reaction zone intensities and heat release rates for these flames occur at the flame base as shown in Figs. 5 and 6, respectively. This suggests that the flames are stabilized at the location of highest reactivity or the reaction kernel as suggested by Takahashi et al. [23]. Generally, both experiments and simulations indicate that as the level of partial premixing is decreased (i.e., as ϕ is increased), the flame liftoff height decreases, whereas the flame length increases. At higher ϕ values, however, the liftoff height becomes nearly independent of ϕ. This aspect is discussed further when we present more quantitative results on the effect of ϕ on flame height. In addition, as ϕ increases, the reaction zones in both 1- and μ-g flames move away from the centerline. Both 1- and μ-g lifted PPFs show that increasing equivalence ratio increases the flame width, as observed in Fig. 5. Another observation from the experimental and predicted results is that the absence of gravity reduces the liftoff height and pushes the flame away from the centerline. Both of these effects can be attributed to the absence of buoyant acceleration (which is clearly shown by the velocity vectors in Fig. 6) in the case of μ-g flames.

To examine the flame structure in the stabilization region more closely, we present the modified flame index contours for the flames discussed in the context of Figs. 5 and 6 in Fig. 7. The utility of using the modified flame index to identify the various reaction zones is clearly illustrated. For all five cases shown in the figure, the 1-g lifted flames exhibit a triple-flame structure at the base, while the corresponding μ-g flames transition from a triple- to a double-flame structure as ϕ increases. Further evidence of different structures at the flame base is provided in Fig. 8, which presents the radial profiles of heat release rate and the CH_4 and O_2 mass fractions at an axial location ($z - L_f^* = 4$ mm) near the flame base for 1-g and

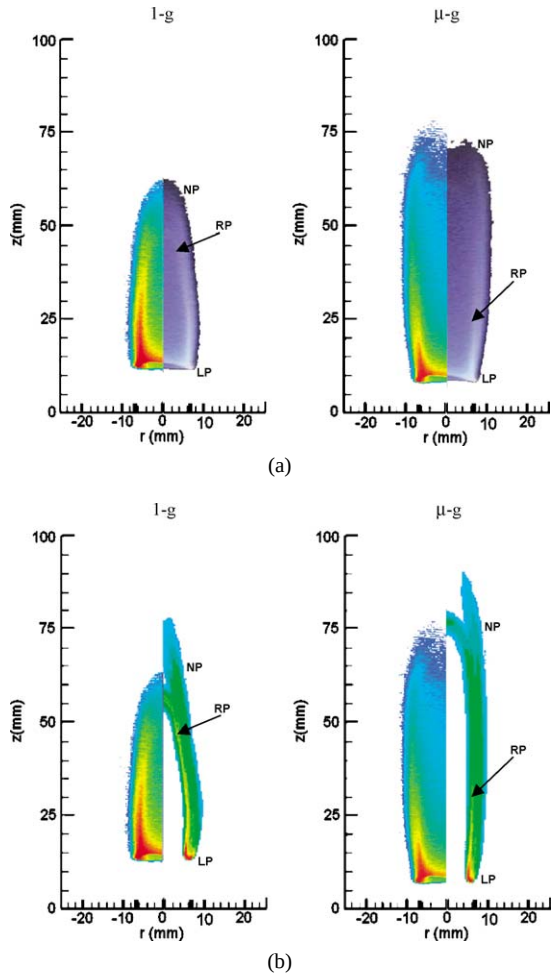

Fig. 3. (a) Original video images (right) and converted flame luminosity intensity contours (left) for lifted 1-g and μ-g PPFs established at $\phi = 2.50$, $V_{in} = V_{out} = 50$ cm/s. (b) Comparison of measured flame luminosity contours (left) and predicted heat release rate contours (right).

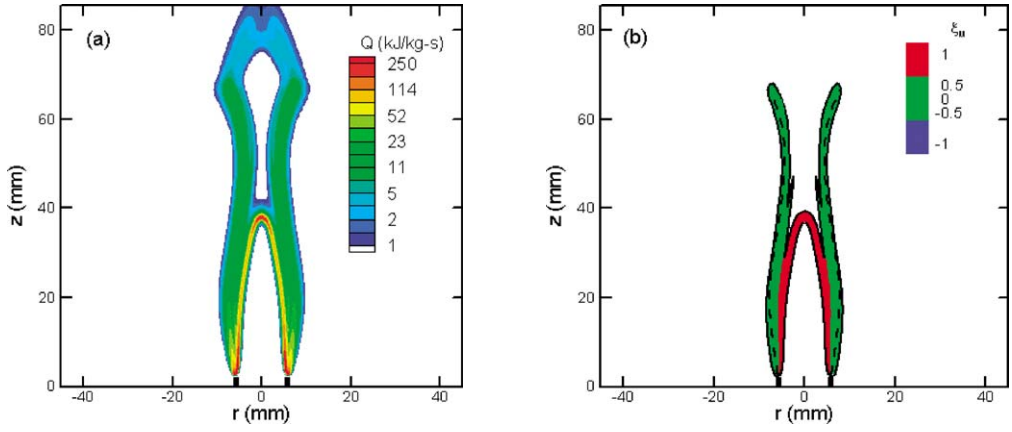

Fig. 4. Predicted (a) heat release rate and (b) modified flame index contours for 1-g PPF established at $\phi = 2.0$, $V_{in} = V_{out} = 50$ cm/s, without nitrogen dilution.

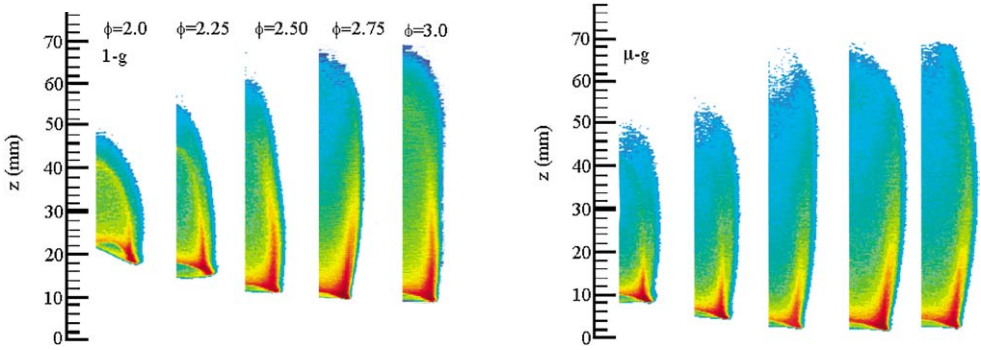

Fig. 5. Images of flame luminosity contours of 1-g and μ-g lifted PPFs at $\phi = 2.00, 2.25, 2.50, 2.75, 3.00$, $V_{in} = V_{out} = 50$ cm/s, and 25% nitrogen dilution.

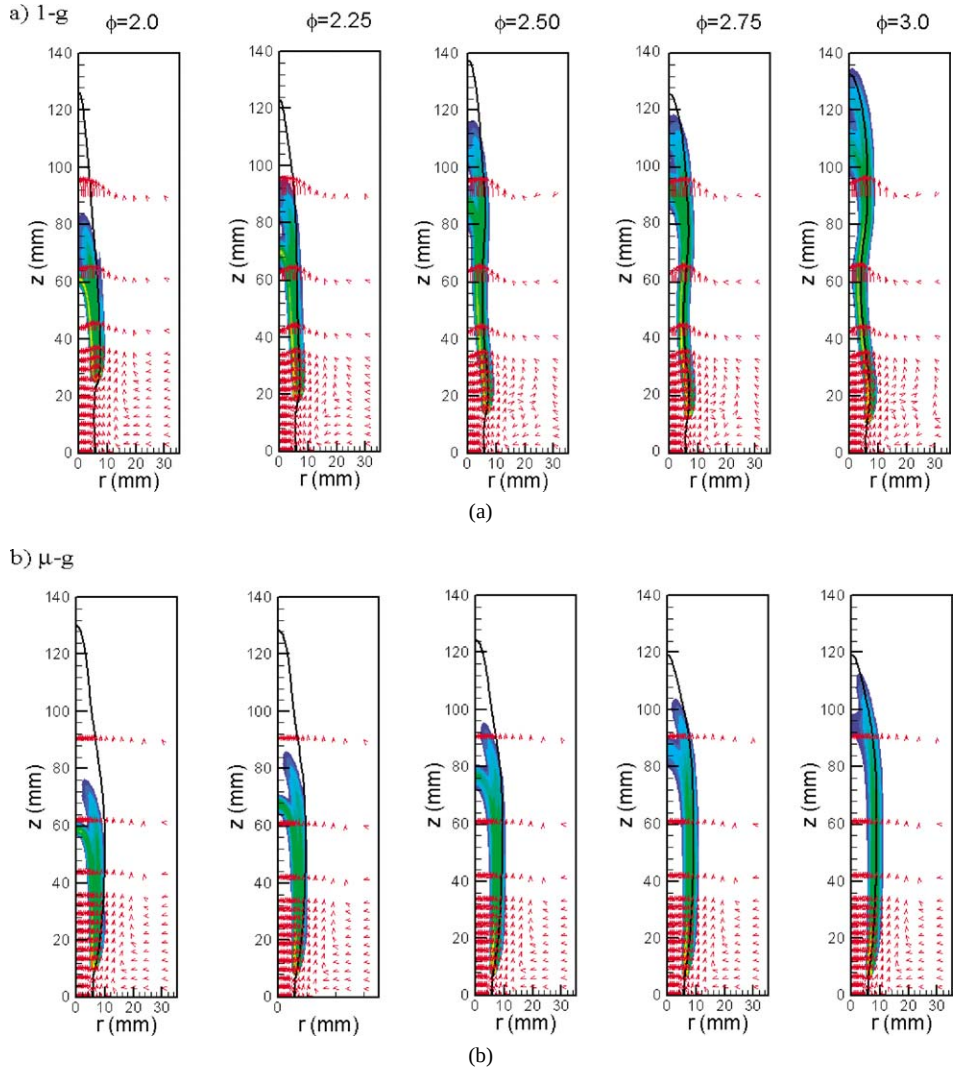

Fig. 6. Predicted heat release rate contours and velocity vector plots for 1-g and μ-g lifted PPFs discussed in the context of Fig. 5. The solid line in each flame represents the stoichiometric mixture fraction, ξ_{st}.

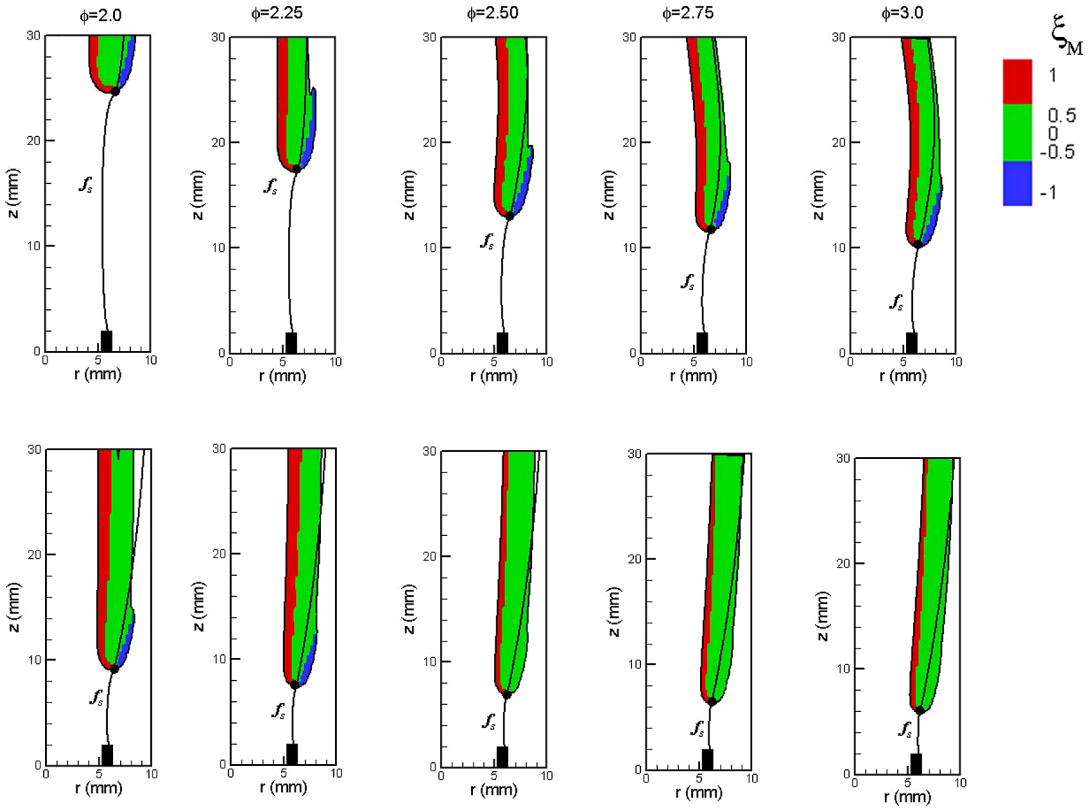

Fig. 7. Modified flame index contours for 1-g and μ-g lifted PPFs discussed in the context of Figs. 5 and 6. The stoichiometric mixture fraction contour is also shown in each flame. The triple point or double point at the flame base is indicated by a solid circle.

μ-g flames established at $\phi = 2.5$ and $V_{in} = V_{out} = 50$ cm/s. Both the heat release rate and CH_4 mass fraction profiles clearly reveal a triple-flame structure for the 1-g flame and a double-flame structure for the μ-g flame. As the 1-g lifted flames are stabilized at a longer distance from the burner than the corresponding μ-g flames, the implication is that the flame base structure strongly depends on the liftoff height. However, altering gravity is not the only way to change the liftoff height, which affects the flame base structure. The liftoff height also depends on the fuel composition, which, in turn, is a function of the fuel type, amount of dilution, and level of partial premixing [25, 39], jet velocity, coflow velocity, nozzle diameter, etc.

Fig. 9 presents the predicted and measured liftoff heights of 1- and μ-g flames as a function of equivalence ratio. The liftoff height in the simulations is measured from the burner exit to the flame base or triple point (which is defined as the intersection of the stoichiometric mixture fraction line and an appropriate scalar contour representing the flame surface [25]). Previous investigations have used a particular value of the fuel mass fraction to identify the flame surface [25,40–42]. In our investigation, the flame surface is defined by the heat release rate contour that corresponds to 1% of $\dot{Q}_{max}$. This contour is chosen so that the results are consistent with the modified flame index discussed in the preceding section. It was difficult to identify the flame base from the experimental video images, and, consequently, the liftoff height is measured from the burner exit to the location of maximum intensity.

There is qualitative agreement between the predicted and measured liftoff heights for both 1- and μ-g flames. Both experiments and simulations indicate that under identical conditions, μ-g lifted PPFs are stabilized closer to the burner compared with the 1-g flames (cf. Figs. 5–7, 9), and the difference in liftoff heights is more pronounced at higher level of partial premixing or lower ϕ. At 1-g, the local flow velocity increases due to buoyant acceleration (cf. Fig. 6) and the flame is stabilized at a higher axial location to balance the flame propagation speed with the local flow velocity. In addition, the entrainment caused by buoyant acceleration leads to larger mixing, which decreases the mixture fraction gradient.

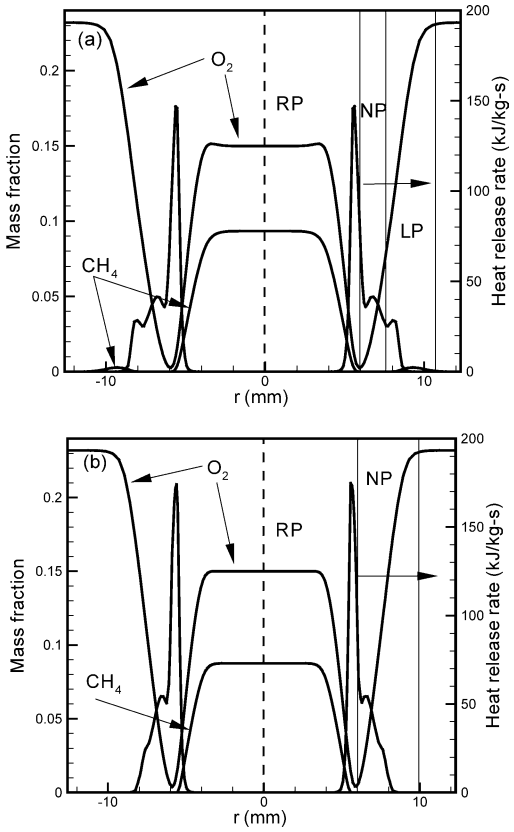

Fig. 8. Radial profiles of heat release rate and CH_4 and O_2 mass fractions at an axial cut ($z - L_f = 4$ mm) for 1-g (a) and μ-g (b) PPFs established at $\phi = 2.50$ and $V_{in} = V_{out} = 50$ cm/s. Reaction zones are indicated by RP (rich premixed), NP (nonpremixed), and LP (lean premixed). Local peaks in the heat release rate correspond to reaction zones.

This, in turn, modifies the flame speed and thereby the liftoff height. On the other hand, the higher liftoff height of 1-g flames induces greater mixing of fuel into the oxidizer stream. Both of these effects, i.e., higher liftoff height and buoyant entrainment, lead to enhanced mixing in the case of 1-g flames. As a result, the 1-g lifted flames exhibit a triple-flame structure at the flame base, while μ-g flames show a transition from a triple- to a double-flame structure. As indicated in Fig. 7, the transition is observed to occur at $\phi = 2.5$, for which the liftoff height is ∼7 mm.

The measurements and simulations also indicate that as ϕ increases, the flame liftoff heights of both 1- and μ-g flames decrease in a nonlinear manner and approach their respective nonpremixed flame limits. As the mixture fraction gradient is increased by decreasing the fuel–air premixing, the thickness of the mixing layer decreases. This, in turn, decreases the flame speed as discussed in Ref. [22]. As mentioned

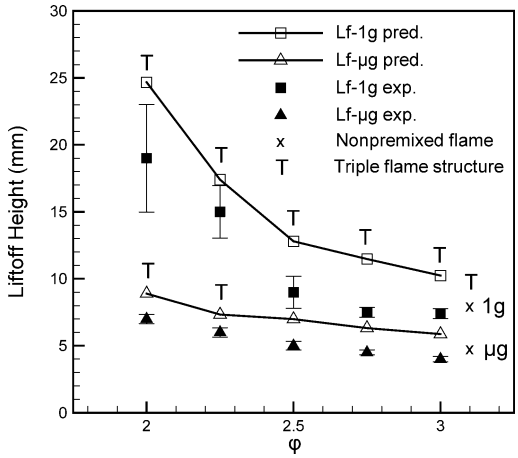

Fig. 9. Measured and predicted liftoff height for the 1-g and μ-g flames as a function of fuel equivalence ratio ϕ. The PPFs are established at $\phi = 2.00, 2.25, 2.50, 2.75, 3.00$, $V_{in} = V_{out} = 50$ cm/s, and 25% nitrogen dilution. The existence of a triple-flame structure in computed flames is indicated by T.

earlier, the flame is stabilized where the local flow velocity matches the flame speed. The minimum liftoff heights thus achieved for the 1- and μ-g nonpremixed flames are 8 and 4.8 mm, respectively, as indicated in Fig. 9. Fig. 10 presents the variation of the flame speed and the local flame stretch at the triple (or "double") point as a function of ϕ for corresponding 1- and μ-g flames. The flame speed S_d, the hydrodynamic stretch κ_h, the curvature-induced stretch κ_c, and the total stretch κ are determined from the relations [43,44]

$$S_d = -\frac{1}{\rho|\nabla\varphi|}\left[\nabla\cdot(\rho D\nabla\varphi) + \omega_\varphi\right],$$

$$\kappa_h = \nabla\cdot V_{fluid} - nn : \nabla V_{fluid},$$

$$\kappa_c = S_d(\nabla\cdot n),$$

and

$$\kappa = \kappa_h + \kappa_c,$$

and are plotted in Fig. 10. As indicated in Fig. 10a, for the 1- and μ-g flames investigated, the total stretch at the flame base is positive and decreases as ϕ is increased. Other important observations from Fig. 10a are that: (1) The curvature-induced stretch κ_c increases while the hydrodynamic stretch κ_h decreases with increasing ϕ. (2) While the total stretch is predominantly due to κ_h at low ϕ, both κ_h and κ_c contribute equally to the total stretch at high ϕ. (3) The curvature-induced stretch is higher for μ-g flames than for 1-g flames, as the μ-g flames are stabilized closer to the burner. In contrast, due to buoyant convection, the hydrodynamic stretch is greater for 1-g flames than for their μ-g counterparts. Consequently, the to-

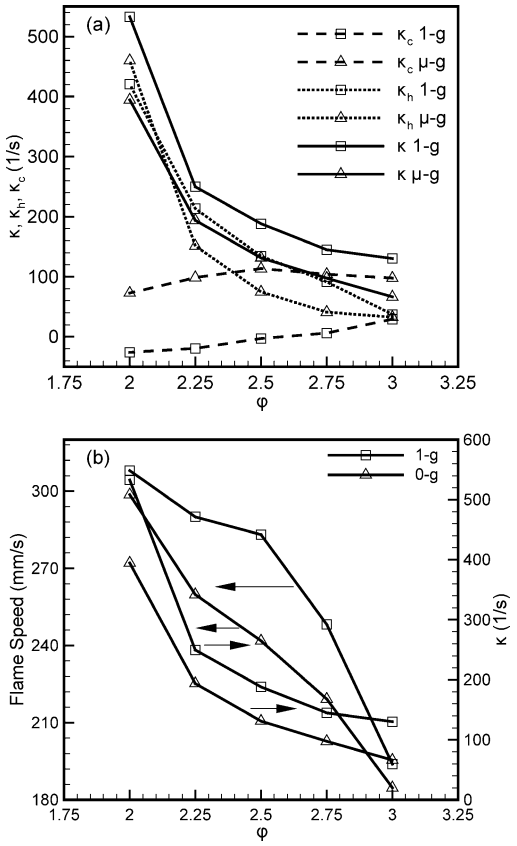

Fig. 10. Predicted curvature-induced stretch (a), hydrodynamic stretch (a), total stretch (a and b), and flame speed (b) at the flame base plotted versus ϕ for the PPFs corresponding to Fig. 9.

tal stretch is higher for 1-g flames. (4) For both 1- and μ-g flames, there is a positive correlation between flame speed and stretch [45,46]. This correlation is further discussed below.

At the triple point (or "double point") the stoichiometric mixture fraction leads to a localized lean mixture, and for lean CH_4/air mixtures, the Lewis number (Le) is less than unity. Thus for the positively stretched flame base, its convex nature toward the fresh mixtures defocuses the heat ahead of the flame, decreasing the burning rate, but focuses the concentration of methane, which increases the burning rate. For Le < 1, the focusing effect dominates, and, therefore, there is a positive correlation between flame speed and stretch. Because the stretch decreases with increasing ϕ, the flame speed (S_d) decreases (cf. Fig. 10b). As S_d decreases, the flame is stabilized closer to the burner exit in order for S_d to match the local flow velocity (cf. Fig. 7). It is important to note that there is a dead zone at the burner rim, and, consequently, the flow velocity increases downstream of the rim.

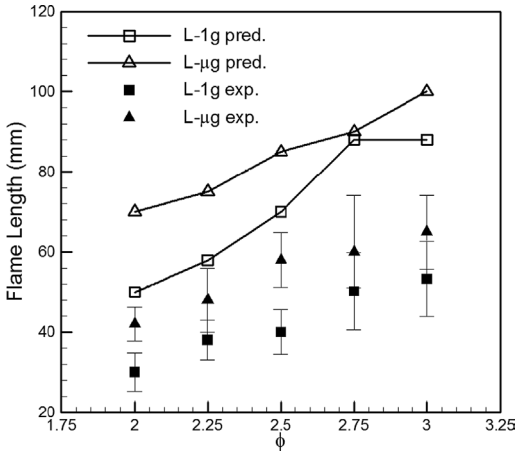

Fig. 11. Measured and predicted flame lengths for 1-g and μ-g lifted PPFs plotted as function of fuel equivalence ratio ϕ. The PPFs are established at $\phi = 2.00, 2.25, 2.50, 2.75, 3.00$, $V_{in} = V_{out} = 50$ cm/s, and 25% nitrogen dilution.

There are quantitative differences between the predicted and measured liftoff heights, especially for 1-g flames at lower ϕ values. The differences between the predicted and measured liftoff heights are similar to those reported by Walsh et al. [47], who conducted an investigation on lifted nonpremixed flames in coflowing jets. The predicted liftoff heights are larger than the measured values. These discrepancies can be attributed to several factors, which include experimental uncertainties, flame asymmetries and unsteadiness in experiments, differences in boundary conditions in the simulations and experiments, and uncertainties in the chemical kinetic mechanism [29]. The experiments show significant unsteadiness in the 1-g lifted flames at lower ϕ values, and, consequently, there is large uncertainty in the measured liftoff heights, as shown in Fig. 9.

4.4. Effect of partial premixing on flame length

Fig. 11 presents the variation of the measured and predicted flame lengths with equivalence ratio for both 1- and μ-g flames. The flame lengths were measured as the distance between the flame base and the nonpremixed reaction zone tip, with the latter based on the intensity contour in the experiments and the centerline reaction rate peak in the simulations. For oscillating flames, an average length was obtained, and for flames with an open tip, the flame length was obtained based on extrapolation. The uncertainty was generally less than 10% in the flame length measurement. The uncertainty was larger for 1-g flames at higher ϕ, because these flames had open tips and were subjected to large-amplitude oscillations due to buoyancy-induced instabilities. Fig. 11 presents good

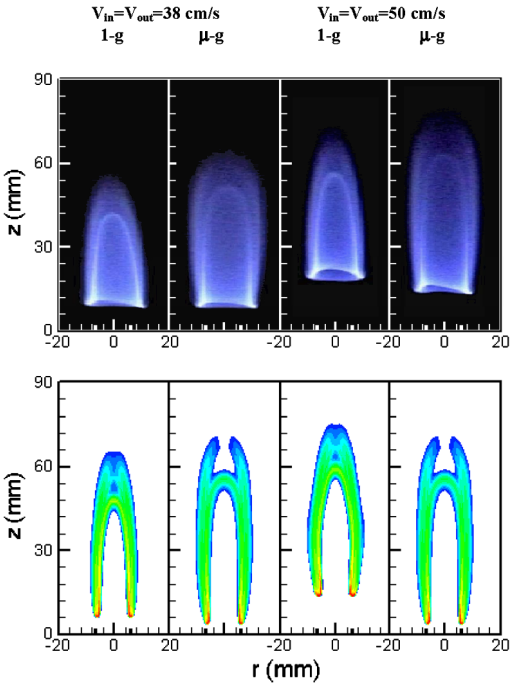

Fig. 12. Measured flame images (top) and predicted heat release rate contours (bottom) for 1-g and μ-g lifted PPFs at $\phi = 2.50$, $V_{\text{in}}/V_{\text{out}} = 38$, and 50 cm/s.

qualitative agreement between the predicted and measured flame lengths, both of which increase as ϕ is increased. However, the predicted flame lengths are larger than the measured values. For both 1- and μ-g flames, the flame length increases as ϕ is increased, because the chemical reaction time increases as the level of partial premixing decreases and, consequently, the flow time increases. In addition, the rich premixed zone has a weaker intensity at higher ϕ values and moves closer to the nonpremixed zone. Under microgravity conditions, the flame length is increased, because the oxidizer transport to the nonpremixed reaction zone is reduced due to the absence of buoyant acceleration, and the effect of radiation increases [1].

4.5. Effect of jet velocity on liftoff height

Fig. 12 presents the experimentally obtained images and the predicted heat release rate contours of 1- and μ-g lifted PPFs established at $\phi = 2.5$ and two different jet velocities ($V_{\text{in}}/V_{\text{out}} = 38$ and 50 cm/s). There is qualitative agreement between experiments and simulations in terms of flame liftoff height, length, and topology. Increasing the jet velocity increases both the flame liftoff height and length. For both 1- and μ-g flames, the liftoff height increases with jet velocity, as the lifted flames are stabilized at higher locations where there is a match between flame speed and local flow velocity. This is expected and consistent with the previous computational and experimental investigations [24,48]. Flame length also decreases because the flow time, which is determined by the chemical reaction time, does not change. Another important observation is that as the liftoff height is sufficiently reduced, there is a transition from a triple-flame structure to a double-flame structure at the flame base, as discussed above.

4.6. Flame oscillations at 1 g

Normal-gravity PPFs exhibit well-organized oscillations in both experiments and simulations. The simulations indicated that the maximum flow velocity is located in the nonpremixed flame wing, suggesting that this wing is oscillating due to buoyant acceleration [49]. Buoyancy-induced flame oscillations in burner-stabilized nonpremixed and partially premixed flames have been extensively investigated previously [1,9,49]. Both computational and experimental studies have reported that the nondimensional frequency associated with these oscillations varies approximately as $\text{Fr}^{0.5}$, where Fr is the Froude number, indicating the ratio of inertial force to gravitational force. For the conditions investigated, our simulations indicated the oscillation frequency for the lifted 1-g PPFs to be in the range of 8–10 Hz, while the measured frequency was found to be in the range 10–15 Hz. However, the video images were recorded at 30 Hz, and, therefore, the frequency was poorly resolved in the measurements. Fig. 13 presents four consecutive images of the experimental and simulated 1-g flames for intervals of 0.13 and 0.15 s, respectively. Therefore, the experimental and simulated images are not exactly at the same phase angle due to differences in their respective frequencies. However, both the measurements and simulations indicate a well-organized flame oscillation. In addition, our results show that while the oscillation frequency is relatively insensitive to ϕ, the oscillation amplitude increases with increasing ϕ, as shown in Fig. 14, which presents the time evolution of flame lengths for different ϕ. This is consistent with our previous investigations on burner-stabilized PPFs, and provides further evidence that the effect of partial premixing (i.e., decreasing ϕ) is to make the flame more stable. In other words, the partially premixed flames are more stable than their corresponding nonpremixed counterparts.

4.7. Effect of radiation on 1-g and μ-g flames

Fig. 15 presents the flame structure in terms of the isotherms for 1-g and μ-g flames simulated with and

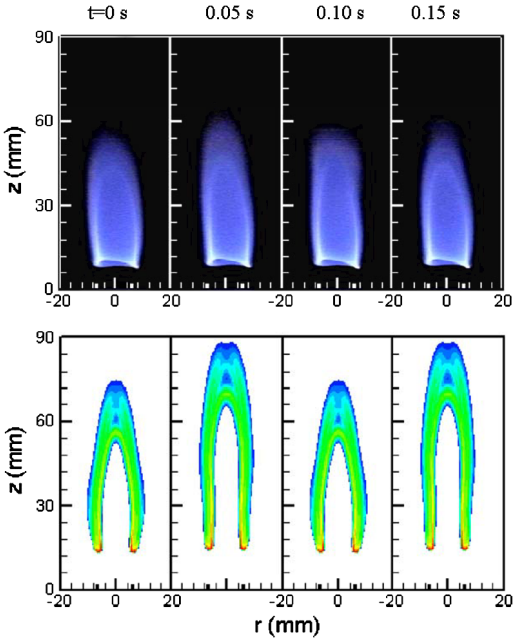

Fig. 13. Sequential flame images (top) and the predicted heat release rate contours (bottom) at different times for a 1-g oscillating flame at $\phi = 2.5$ and $V_{in} = V_{out} = 50$ cm/s.

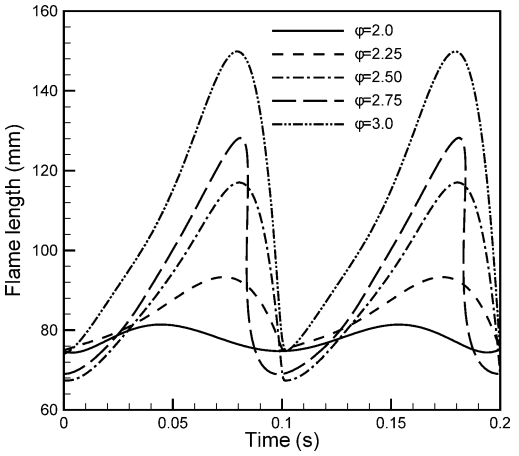

Fig. 14. Time evolution of flame lengths for 1-g lifted PPFs at $\phi = 2.00, 2.25, 2.50, 2.75, 3.00$, $V_{in} = V_{out} = 50$ cm/s, and 25% nitrogen dilution.

without radiation. These contours show that the liftoff heights of both 1- and μ-g PPFs slightly decrease when radiation is included. This can be attributed to the fact that thermal radiation lowers the local temperature, which reduces the flame speed, and, consequently, the flame is stabilized closer to the burner. For the 1- and μ-g flames depicted in Fig. 15, the liftoff heights decrease by 6.4 and 6.8%, respectively. As expected, radiation also decreases the temperature in the high-temperature regions. Overall, the effect of

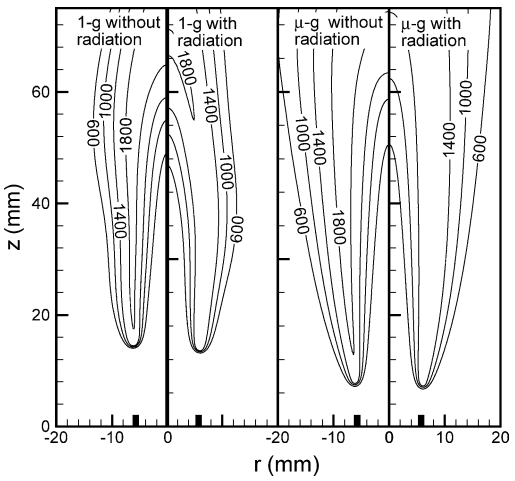

Fig. 15. Temperature contours for 1-g and μ-g lifted PPFs computed with and without radiation. Flames are established at $\phi = 2.50$, $V_{in} = V_{out} = 50$ cm/s, and 25% nitrogen dilution.

radiation is slightly larger for μ-g flames. This is consistent with our previous investigation pertaining to burner-stabilized PPFs [9], which indicated that without a coflow the effect of radiation is significantly larger for μ-g flames as compared with 1-g flames. However, with a coflow, this effect is significantly reduced.

5. Conclusion

We have presented an experimental and computational investigation on the liftoff characteristics of partially premixed flames under 1- and μ-g conditions. Lifted methane–air PPFs have been established in axisymmetric coflowing jets using nitrogen dilution. The μ-g experiments have been conducted in the 2.2-s drop tower facility at the NASA Glenn Research Center. A time-accurate, implicit algorithm that uses a detailed description of methane–air chemistry and includes radiation effects is used for simulations. Predictions are validated through a comparison of the flame reaction zone topologies, liftoff heights, flame lengths, and oscillation frequencies. The effects of equivalence ratio, gravity, jet velocity, and radiation are discussed.

1. Both the simulations and measurements indicate that under identical conditions, a lifted μ-g PPF is stabilized closer to the burner compared with the 1-g flame, and the difference in liftoff heights is more pronounced at lower ϕ values. At 1-g, the local flow velocity increases due to buoyant acceleration, and the 1-g flame is stabilized at a higher axial location

to achieve a balance between flame speed and local flow velocity. The higher liftoff height and entrainment caused by buoyant acceleration lead to enhanced mixing for 1-g flames. As a result, 1-g lifted flames exhibit a triple-flame structure at the base, while μ-g flames show a transition from triple-flame to double-flame structure.

2. For the 1- and μ-g flames investigated, the total stretch at the flame base is positive and decreases as ϕ is increased. While the curvature-induced stretch increases and the hydrodynamic stretch decreases with increasing ϕ, the total stretch is generally dominated by the latter. In addition, the total stretch is higher for 1-g flames than for μ-g flames. For both 1- and μ-g flames, there is a positive correlation between flame speed and total stretch, and this can be attributed to the fact that these flames are positively stretched and the local Lewis number at the triple (or "double") point is less than unity.

3. The liftoff heights of both 1- and μ-g flames decrease with increasing ϕ, and approach their respective nonpremixed flame limits. This is related to the effect of ϕ on the flame speed at flame base. As ϕ increases, the flame stretch decreases, and therefore, the flame speed decreases. Consequently, the flame is stabilized closer to the burner exit in order for the flame speed to match the local flow velocity. Similarly, the liftoff heights for these flames decrease with decreasing jet velocity because the flame is stabilized at the location where the local flow velocity matches the flame speed.

4. The 1-g lifted flames exhibit well-organized oscillations due to a buoyancy-induced instability while the corresponding μ-g flames exhibit steady-state behavior. The oscillation frequency is about 10 Hz, and is essentially independent of ϕ. However, oscillation amplitude increases with increasing ϕ.

5. The effect of radiation is to slightly decrease the liftoff heights of both 1-g and μ-g flames, and reduce the temperature in the high-temperature regions.

6. A modified flame index is developed to clearly distinguish between the rich premixed, lean premixed, and nonpremixed reaction zones near the flame base.

In future investigations, we plan to use lifted PPFs to study different flame suppression scenarios, for example, the evaluation of different fuel fire suppressants (such as CO_2) in extinguishing flames at different gravity levels.

Acknowledgments

This research was supported by the NASA Microgravity Research Division through Grant NCC3-688 for which Dr. Kurt Sacksteder serves as the technical monitor. Andrew Lock was supported by a fellowship through the NASA Graduate Student Research Program.

References

[1] Z. Shu, S.K. Aggarwal, V.R. Katta, I.K. Puri, Combust. Flame 111 (1997) 276–295.
[2] R. Azzoni, S. Ratti, I.K. Puri, S.K. Aggarwal, Phys. Fluids 11 (1999) 3449–3464.
[3] Y. Hardalupas, M. Orain, C.S. Panoutsos, A.M.K.P. Taylor, J. Olofsson, H. Seyfried, M. Richter, J. Hult, M. Aldén, F. Hermann, J. Klingmann, Appl. Therm. Eng. 24 (2004) 1619–1632.
[4] F.F. Flynn, R.P. Durrett, G.L. Hunter, A.O. zur Loyer, O.C. Akinyemi, J.E. Dec, C.K. Westbrook, Diesel Combustion: An Integrated View Combining Laser Diagnostics, Chemical Kinetics, and Empirical Validation, SAE paper 99-01-0509, 1999.
[5] A. Hammis, K. Konishi, P. Borthwick, T. Kashiwagi, Proc. Combust. Inst. 26 (1996) 1429.
[6] K.R. Sacksteder, Proc. Combust. Inst. 23 (1990) 1589.
[7] C.K. Law, G.M. Faeth, Prog. Energy Combust. Sci. 20 (1994) 65–113.
[8] A.J. Lock, R. Ganguly, I.K. Puri, S.K. Aggarwal, U. Hedge, Proc. Combust. Inst. 30 (2004) 511–518.
[9] X. Qin, I.K. Puri, S.K. Aggarwal, V.R. Katta, Phys. Fluids 16 (2004) 2963–2974.
[10] N. Peters, F.A. Williams, AIAA J. 21 (1983) 423–429.
[11] W.M. Pitts, Proc. Combust. Inst. 22 (1988) 809–816.
[12] S.H. Chung, B.J. Lee, Combust. Flame 86 (1991) 62–72.
[13] B.J. Lee, S.H. Chung, Combust. Flame 109 (1997) 163–172.
[14] P.N. Kioni, B. Rogg, K.N.C. Bray, A. Liñán, Combust. Flame 95 (1993) 276–290.
[15] L. Vervisch, Proc. Combust. Inst. 28 (2000) 11–24.
[16] S. Ghosal, L. Vervisch, Combust. Flame 123 (2001) 646–655.
[17] A. Liñán, in: J. Buckmaster, T.L. Jackson, A. Kumar (Eds.), Combustion in High Speed Flows, Kluwer Academic, Boston, 1994, p. 461.
[18] T. Plessing, P. Terhoeven, N. Peters, M.S. Mansour, Combust. Flame 115 (1998) 335–353.
[19] T. Echekki, J.H. Chen, Combust. Flame 114 (1998) 231–245.
[20] L. Muniz, M.G. Mungal, Combust. Flame 111 (1997) 16–30.
[21] I.K. Puri, S.K. Aggarwal, R. Azzoni, S. Ratti, Combust. Flame 124 (2001) 311–325.
[22] G.R. Ruetsch, L. Vervisch, A. Liñán, Phys. Fluids 7 (1995) 1447–1454.
[23] F. Takahashi, W.J. Schmoll, V.R. Katta, Proc. Combust. Inst. 27 (1998) 675–684.
[24] N.I. Kim, J.I. Seo, K.C. Oh, H.D. Shin, Proc. Combust. Inst., in press.
[25] X. Qin, I.K. Puri, S.K. Aggarwal, Proc. Combust. Inst. 29 (2002) 1565–1572.
[26] H.N. Najm, P.H. Paul, C.J. Mueller, P.S. Wyckoff, Combust. Flame 113 (1998) 312–332.

[27] V.R. Katta, L.P. Goss, W.M. Roquemore, Combust. Flame 96 (1994) 60–74.
[28] R. Siegel, J.R. Howell, Thermal Radiation Heat Transfer, Hemisphere, New York, 1981.
[29] N. Peters, Reduced Kinetic Mechanisms for Applications in Combustion Systems, in: N. Peters, B. Rogg (Eds.), Lecture Notes in Physics, vol. m15, Springer-Verlag, Berlin, 1993, pp. 3–14.
[30] Z. Shu, C. Choi, S.K. Aggarwal, V. Katta, I.K. Puri, Combust. Flame 118 (1999) 91–107.
[31] X. Qin, I.K. Puri, S.K. Aggarwal, Phys. Fluids 40 (2001) 731–740.
[32] H. Xue, S.K. Aggarwal, AIAA J. 39 (2001) 637–645.
[33] Z. Shu, B. Krass, C. Choi, S.K. Aggarwal, V. Katta, I.K. Puri, Proc. Combust. Inst. 27 (1998) 625–632.
[34] H. Yamashita, M. Shimada, T. Takeno, Proc. Combust. Inst. 26 (1996) 27–34.
[35] P. Domingo, L. Vervisch, J. Réveillon, Combust. Flame 140 (2005) 172–195.
[36] S.K. Aggarwal, I.K. Puri, AIAA J. 36 (1998) 1190–1199.
[37] R.W. Bilger, Proc. Combust. Inst. 22 (1988) 475–488.
[38] A.M. Briones, S.K. Aggarwal, Int. J. Hydrogen Energy 30 (2005) 327–339.
[39] S.H. Won, S.H. Chung, M.S. Cha, B.J. Lee, Proc. Combust. Inst. 28 (2000) 2093–2099.
[40] H.N. Najm, P.S. Wyckoff, Combust. Flame 110 (1997) 92–112.
[41] L.P.H. De Goey, R.M.M. Mallens, J.H.M. Ten Thije Boonkkamp, Combust. Flame 110 (1997) 54–66.
[42] H.G. Im, J.H. Chen, Combust. Flame 119 (2002) 436–454.
[43] X. Qin, C.W. Choi, A. Mukhopadhyay, I.K. Puri, S.K. Aggarwal, V.R. Katta, Combust. Theory Model. 8 (2004) 293–314.
[44] A. Mukhopadyay, I.K. Puri, Combust. Flame 133 (2003) 499–502.
[45] C.W. Choi, I.K. Puri, Combust. Flame 126 (2001) 1640–1654.
[46] C.K. Law, C.J. Sung, Prog. Energy Combust. Sci. 26 (2000) 459–505.
[47] K.T. Walsh, J. Fielding, M.D. Smooke, M.B. Long, A. Liñán, Proc. Combust. Inst., in press.
[48] J. Lee, S.H. Chung, Combust. Flame 127 (2001) 2194–2204.
[49] S.H. Won, J. Kim, M.K. Shin, S.H. Chung, O. Fujita, T. Mori, J.H. Choi, K. Ito, Proc. Combust. Inst. 29 (2002) 37–44.